Numerical simulations of viscoelastic flows with free surfaces

Comminal, Raphaël Benjamin; Spangenberg, Jon; Hattel, Jesper Henri

Published in:
21ème Congrès Français de Mécanique

Publication date:
2013

Numerical simulations of viscoelastic flows with free surfaces

R. COMMINAL[a], J. SPANGENBERG[b], J.H. HATTEL[a]

a. *Technical University of Denmark (DTU), Produktionstorvet, 2800 KGS. LYNGBY (DENMARK)*
b. *Princeton University, PRINCETON, NJ 08540 (USA)*

Résumé :

Nous présentons une méthodologie pour simuler les écoulements viscoélastiques possédant des surfaces libres, dans la perspective de modéliser les procédés de mise en forme des polymères, tels que l'extrusion ou le moulage par injection. L'utilisation de lois de comportements viscoélastiques permet de prendre en compte les "effets de mémoire" des polymères déformés. Cependant, leurs utilisations engendrent aussi des difficultés d'ordre numériques, que nous résolvons avec une reformulation des contraintes viscoélastiques par la "log-conformation-transformation". Par ailleurs, la nouveauté de ces travaux réside dans l'utilisation de la méthode dite des "volume-of-fluid" pour simuler le déplacement des surfaces libres du fluide viscoélastique. Enfin, nous présentons des résultats de simulations préliminaires où nous testons séparément les différentes possibilités de notre modèle.

Abstract:

We present a new methodology to simulate viscoelastic flows with free-surfaces. These simulations are motivated by the modelling of polymers manufacturing techniques, such as extrusion and injection moulding. One of the consequences of viscoelasticity is that polymeric materials have a "memory" of their past deformations. This generates some numerical difficulties which are addressed with the log-conformation transformation. The main novelty of this work lies on the use of the volume-of-fluid method to track the free surfaces of the viscoelastic flows. We present some preliminary results of test case simulations where the different features of the model are tested independently.

Key words: computational rheology, viscoelastic flows, free-surface flows, volume-of-fluid method

1 Introduction

The simulation of viscoelastic flows with free surfaces is of particular interest for the modelling of polymer processing technologies, such as extrusion, injection moulding, blow moulding and tape casting, of single polymeric materials and ceramics colloidal suspension. Polymer solutions and melts are known for their non-Newtonian behaviours: *shear-thinning* (when the viscosity decreases with the deformation-rate), and *viscoelasticity* (when the deformations are affected by memory effects). Viscoelasticity is responsible for stress relaxation, creep deformations and elastic drawback. Those non-Newtonian behaviours fundamentally arise from the complex microstructure of the material, where long polymer chains are able to slide between each other, get stretched and change conformations during the deformations [1]. Non-Newtonian effects can also cause viscous and elastic interfacial instabilities in stratified flows [2]. This issue is important from both theoretical and practical points of views, especially for the co-processing of multi-material architectures.

Historically, the first studies of viscoelastic flows with free-surfaces were using Lagrangian methods (based on deforming meshes) in the context of finite-element analysis, to investigate the extrudate swell problem [3]. More recently, the *marker-and-cell* method [4] and the *level set* method [5] were implemented in order to track the free surfaces. Mixed Eulerian-Lagrangian methods were also developed [6]. In the present work, we use the *volume-of-fluid* (VOF) method, in which the free-surfaces are represented in a purely Eulerian manner. The main advantage of Eulerian methods over the Lagrangian methods is that they can adapt to arbitrary changes of topology of the free surfaces [7]. This is a very important feature for the simulation of injection moulding of complex geometries, in which junctions and separations of the material front frequently happen.

In the first part of the paper, we present the governing equations of the model. Then, the specific numerical techniques used to solve the viscoelastic flow problem and the free surfaces are briefly described. Each of those techniques has been implemented and tested separately with various test-case simulations. Finally, concluding remarks are summarized at the end of the paper.

2 Governing equations

The basic equations to be solved are the *continuity equation* (conservation of mass):

$$\nabla \cdot (\rho \boldsymbol{u}) = 0 \tag{1}$$

and the *momentum equations* (conservation of linear momentum):

$$\frac{\partial \rho \boldsymbol{u}}{\partial t} + \nabla \cdot (\rho \boldsymbol{u}\boldsymbol{u}) = -\nabla p + \mu \nabla^2 \boldsymbol{u} + \nabla \cdot \boldsymbol{\sigma} \tag{2}$$

where ρ is the bulk density, μ is the (Newtonian) viscosity of the material, $\boldsymbol{u}$ is the velocity vector, p is the isostatic pressure and $\boldsymbol{\sigma}$ is the viscoelastic extra-stress tensor. In order to close this system of equations, a *constitutive model* which relates the viscoelastic stress tensor to the kinetics of the flow is required. The specificity of viscoelastic materials is that they behave both like liquids (viscous deformation) and solids (elastic deformation), depending on the time scale of observation or their rates of deformation. As a consequence, viscoelastic constitutive models cannot be expressed with algebraic relations, like for purely viscous and purely elastic materials. Indeed, viscoelastic constitutive models are either written on integral form or as partial differential equations (PDE), with respect to time. A large variety of models exist within those two classes of constitutive relations. On the one hand, some models were developed from an empirical approach, in order to fit particular experimental data best. On the other hand, generic models with the capability of describing most standard flow behaviours were derived, either from molecular kinetic theories or pure mathematical expansions [8]. In general, the appropriate constitutive model should be chosen considering its simplicity, its computational efficiency, its flexibility and its capability to describe the expected flow features. In this work, we use the *Oldroyd-B* model, which is one of the most popular viscoelastic constitutive relations. It is a linear partial differential constitutive model:

$$\lambda \frac{\mathfrak{D}\boldsymbol{\sigma}}{\mathfrak{D}t} + \boldsymbol{\sigma} = \eta \dot{\boldsymbol{\gamma}} \tag{3}$$

where λ is the relaxation time of the material, η is the viscosity of the viscoelastic deformations, $\dot{\boldsymbol{\gamma}} = \nabla \boldsymbol{u} + (\nabla \boldsymbol{u})^{\mathrm{T}}$ is the strain-rate tensor, and

$$\frac{\mathfrak{D}\boldsymbol{\sigma}}{\mathfrak{D}t} = \frac{d\boldsymbol{\sigma}}{dt} + \boldsymbol{u} \cdot \nabla \boldsymbol{\sigma} - (\nabla \boldsymbol{u})^{\mathrm{T}} \cdot \boldsymbol{\sigma} - \boldsymbol{\sigma} \cdot (\nabla \boldsymbol{u}) \tag{4}$$

is the upper-convected time derivative of the stress tensor.

3 Numerical methods

3.1 Discretisation

The governing equations are discretized in space with the Eulerian finite-volume method. The calculation domain is divided in non-overlapping control volumes (CV), forming a structured orthogonal mesh of the geometry. The pressure and the viscoelastic stress component are stored at the centre of the CV, while the different velocity components stored at the centres of boundaries of the CV, as represented in figure 1(a). This staggered arrangement of the variables avoids the odd-even pressure decoupling. The equations of conservation (of mass and linear momentum) are integrated on each CV, and expressed in terms of a flux balance, via the divergence theorem. The evaluation of the fluxes at the boundary of the CV requires an interpolation. We use a quadratic upwind interpolation scheme with second-order accuracy in space. Moreover, the boundedness of interpolation is insured by the use of flux limiters, enhancing the stability of the scheme [9]. The resulting PDEs are further discretized in time with the two-step backward differentiation formula (BDF2), and the non-linear convective terms are linearized with a Taylor expansion around the solution at the previous time-step. It results in a stable implicit scheme with second-order accuracy in time.

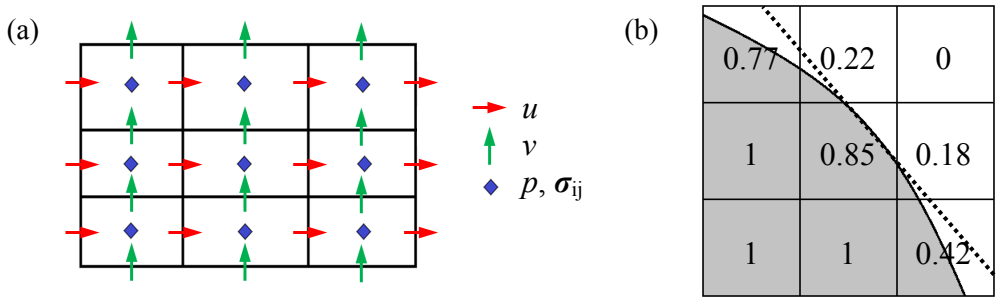

FIG. 1 – (a) Staggered variable arrangement on the mesh and (b) geometrical reconstruction of the free surface with a piecewise linear function.

The dimensionless quantity commonly used to measure the effect of viscoelasticity is the *Weissenberg number Wi*, defined as $Wi = \lambda\dot{\gamma}$, where $\dot{\gamma}$ is a characteristic deformation rate of the flow. When elastic effects are dominant (at high *Wi*), the solution of the constitutive equation is a fast exponential decay. It is a typical "stiff problem" prone to numerical instability. This difficulty is known as the « *High Weissenberg Number Problem* » [10]. It can be remedied by the passage to logarithmic variables in the constitutive equation [11,12]. It is done by taking the matrix-logarithm of the conformation tensor

$$\boldsymbol{c} = \boldsymbol{I} + \frac{\lambda}{\eta}\boldsymbol{\sigma} \tag{5}$$

because it is always *symmetric-positive-definite* (at the contrary to the viscoelastic stress tensor), which is a necessary condition for the existence of the matrix-log. The matrix-logarithm transformation also required the diagonalisation of the conformation tensor:

$$\log(\boldsymbol{c}) = \boldsymbol{R}\log(\boldsymbol{\Lambda})\boldsymbol{R}^{\mathrm{T}} \tag{6}$$

where $\boldsymbol{\Lambda}$ is a diagonal matrix containing the eigenvalues of the conformation tensor, and $\boldsymbol{R}$ is the orthogonal matrix of the eigendecomposition. This transformation yields a conservation equation for the log-conformation tensor $\boldsymbol{\Theta} = \log(\boldsymbol{c})$, which has a linear decay as solution. Without this transformation, the calculation of viscoelastic flows is still possible, but it is limited to *Wi* numbers below a threshold value depending on the kinetics of the flow and the discretisation techniques [13]. The results presented in the next section have been obtained without the use of the log-conformation transformation, in flow configurations below this limit.

3.2 Solution procedure

The velocities and the viscoelastic stresses can be calculated separately, by solving the momentum and constitutive equations sequentially. However, we do not have an evolution equation for the pressure, which is only seen in the momentum equations. The pressure is determined through the combination of the momentum and continuity equations instead. Indeed, the pressure can be seen as a Lagrange multiplier of the continuity equation, which limits the solution of the velocity to a divergence-free vector field. Therefore, the momentum and continuity equations have to be solved at the same time, but it is challenging from a numerical point of view, because the Jacobi matrix of the discretised system of equations is ill-conditioned. As a consequence, the numerical solutions are inaccurate and expensive to compute since only direct solvers, e.g. Gaussian elimination, can be used. The approach to remedy this problem is to derive a separate equation for the pressure, by taking the divergence of the momentum equations (the Chorin-Temam method). The resulting system of equations is further decoupled using a generalised LU-block decomposition [14]. We solve the problem efficiently with the GMRES iterative solver, based on conjugated-gradients.

3.3 Free surfaces tracking

Within the VOF method, a new discrete variable is introduced: the volume fraction $0 \leq \varphi \leq 1$ of the control volumes. At the end of each time step, the volume fraction is transported explicitly with the flow, and the apparent material properties of the CV are updated with the rule of mixture accordingly. The capillary forces

(surface tension) are neglected, as in this case they are several orders of magnitude lower than the viscous and elastic stresses. The advection scheme of the VOF method conserves the mass, and consists of two steps:

- The *geometrical reconstruction*: the interface inside cells where $0 < \varphi < 1$ is represented by a piecewise linear function. The position of the interface is parameterized by two variables: its slope and its distance from the centre of the control volume; and has one constraint: the volume fraction inside the cell. The remaining free parameter is determined so that the prolongation of the piecewise linear function into the eight neighbouring cells (in 2D) fits the best their volume fractions, see figure 1(b). This consists in an optimization problem. We use the ELVIRA method [15], which evaluates only six candidates for the interface, and chose the one which minimise the least-square error, without iterations. This method is of second-order accuracy.
- The *forward advection scheme*: the volume fraction of the fluid is advected explicitly, using the reconstructed position of the interface to evaluate the conservative fluxes. The volume fractions which are exchanged with the neighbouring cells are the one of the volumes effectively donated/accepted, rather than the total one of the cells. The time-step size of the calculation is constrained by the *Courant–Friedrichs–Lewy condition*, but the numerical diffusion of the scheme is limited. We used a split advection, and alternate the order of the directions of advection at every time-step. It was shown in [15] that in this way the advection is second-order accurate in time.

Unlike the front-tracking methods using markers or continuous chain of line segments to represent the interfaces, the VOF method naturally handles the junctions and separations of surfaces, without any need of surgical operations adding or removing boundary elements [7].

4 Results

This section presents the results of preliminary simulations performed in order to validate the implementation of our methods. The first test-case simulation is the transient viscoelastic Poiseuille flow driven by a pressure gradient suddenly imposed at the initial time. This simulation is used to validate the temporal accuracy of the algorithm, as it is one of the few transient problems for which an analytical solution exists. The exact solution does not have a closed form and is expressed as an infinite series, see [16]. The numerical simulation is performed at $Re = 0.02$, $Wi = 0.3$ and $\eta/\mu = 0.75$. Figure 2 presents the velocity magnitude at the central line of the channel, as well as the velocity profiles at different points of time. Unlike purely viscous fluids, here the velocity profile growths until it reaches a maximal amplitude, and then decrease slowly due to viscoelastic effects. The numerical results are in very good agreements with the analytical solution, and confirm the good temporal accuracy of the BDF2 scheme.

The second test-case simulation is the steady-state viscoelastic flow in planar contraction-expansion geometry. The flow inlet and outlet are the west and east boundaries of the domain respectively, where fixed pressures are imposed. The south boundary is a symmetry line, and all the other boundaries are solid walls with the no-slip condition. Flows in planar contraction have already been investigated, both theoretically [17,18] and numerically [19,20]. It was notably used to assess the spatial accuracy of different interpolation schemes [9,13]. Indeed, the different components of the velocity vector and the viscoelastic stress tensor are strongly coupled; the flow exhibits vortices at the salient corners, and stress singularities at the reentrent corners. However, the use of a staggered mesh arrangement avoids the calculation of the stress singularities. Figure 3 displays the contour plots of the pressure level and the viscoelastic stresses for a creeping flow ($Re = 0$) at $Wi = 1.04$ with $\eta/\mu = 1$. Unlike for purely viscous fluids, the viscoelastic creeping flow is unsymmetrical because of to the memory effects.

The last test-case simulation is the extrusion of a Newtonian fluid with free surfaces at $Re = 0$. The position of the free surface at the end of the extrusion is represented in the figure 4. The swelling ratio, defined as the ratio of the diameter of the extrudate by the diameter die, is $R_d/R_e = 1.45$. In this case, the swelling is due to dynamical effects only, as Newtonian fluids do not have memory effects. Indeed, the velocity profile, which has a parabolic shape at the die exit, has to rearrange itself to become a homogeneous velocity profile. We observe that it takes a distance of approximately $3R_d$ from the die exit for the material to obtain its final diameter. This simulation demonstrates the ability of the VOF method to track the free-surface in extrusion.

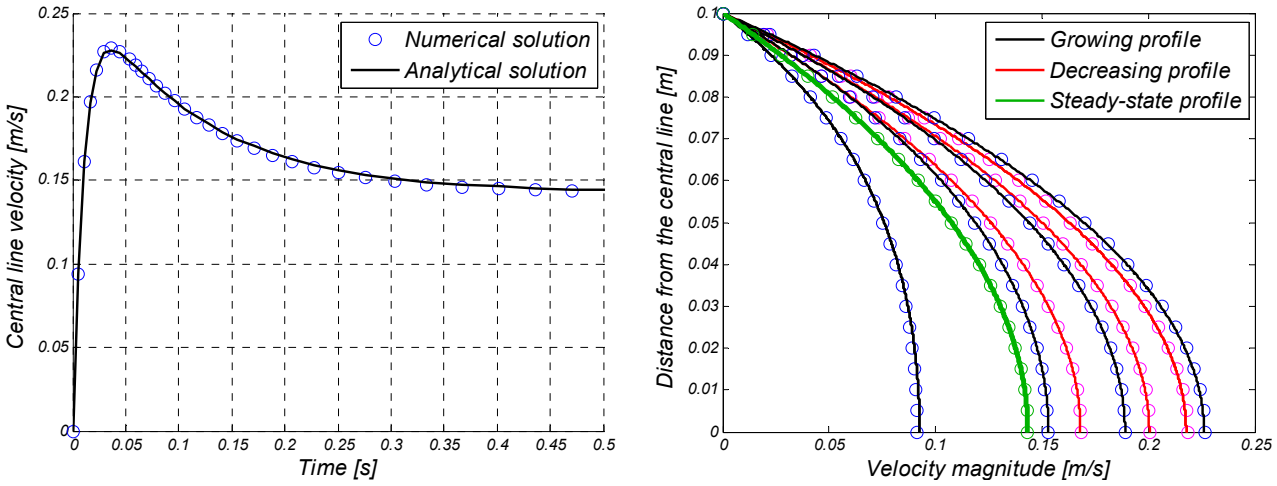

FIG. 2 – Transient viscoelastic Poiseille flow at $Re = 0.02$, $Wi = 0.3$ and $\eta/\mu = 0.75$. Left: velocity magnitude at the central line of the channel. Right: velocity profiles at the times [sec]: 0.005, 0.01, 0.015 (growing velocity profiles), 0.03, 0.09, 0.18 (decreasing velocity profiles), and 0.6 (steady-state solution).

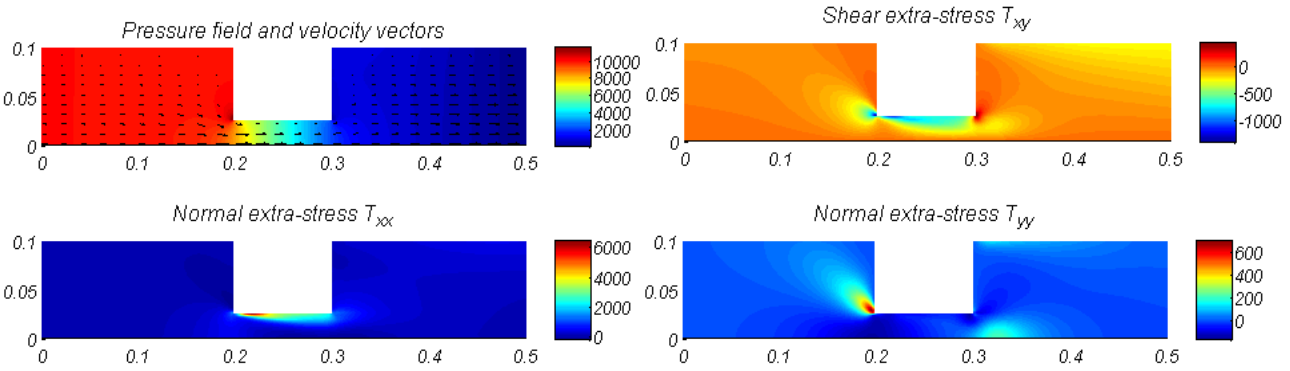

FIG. 3 – Contour plot of the pressure level and the viscoelastic stresses for the viscoelastic creeping flow in the planar contraction-expansion geometry at $Wi = 1.04$ with $\eta/\mu = 1$.

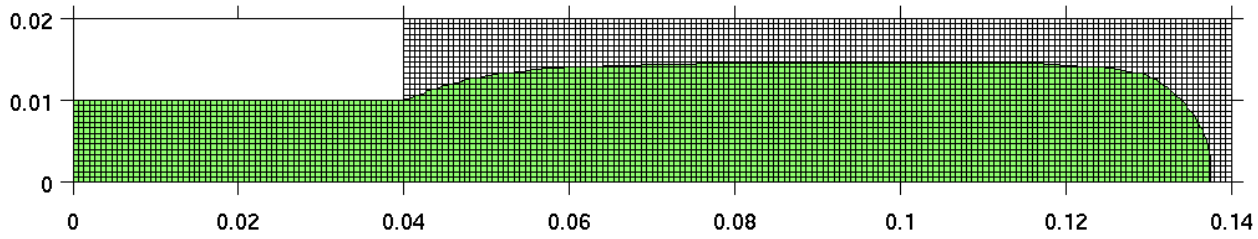

FIG. 4 – Position of the free surface at the end of the extrusion of a Newtonian material at $Re = 0$.

5 Concluding remarks

A numerical framework for the modelling of viscoelastic flows with free surfaces has been presented. The different features of the model: the viscoelastic stress solver and the free surface tracking algorithm, were tested separately. Their coupling has not been done yet, and it will be the focus of our future work. The preliminary results show good temporal and spatial resolutions, thanks to the second-order accuracy of the BDF2 and the upwind quadratic interpolation schemes. Moreover, the VOF method is a robust technique to track the free surfaces of viscoelastic flows, since it can adapt to changes of topology of the free surfaces. This is of great interest for the simulation of polymers manufacturing processes. This method can also be used to predict the interface deformations, due to the flow instability and the secondary recirculation flows generated by viscoelastic effects, in the co-processing of multi-materials architectures.

Acknowledgements

The authors would like to acknowledge the support of the Scientific Research Councils on Technology and Production Sciences (FTP) (Contract No. 09-072888, OPTIMAC), which is part of the Danish Council for Independent Research (DFF).

References

[1] Larson R.G., Constitutive Equations for Polymer Melts and Solutions, 1988.
[2] Dooley J., Hyun K.S., Hughes K., An experimental study on the effect of polymer viscoelasticity on layer rearrangement in coextruded structures, Polymer Engineering and Science, 38, 1060-1071, 1998.
[3] Crochet M.J., Keunings R., Finite element analysis of die swell of a highly elastic fluid, Journal of Non-Newtonian Fluid Mechanics, 10, 339-356, 1982.
[4] Tomé M.F., Mangiavacchi N., Cuminato J.A., Castelo A., McKee S., A finite difference technique for simulating unsteady viscoelastic free surface flows, Journal of Non-Newtonian Fluid Mechanics, 106, 61-106, 2002.
[5] Pillapakkam S.B., Singh P., A level-set method for computing solutions to viscoelastic two-phase flow, Journal of Computational Physics, 174, 552-578, 2001.
[6] Bonito A., Picasso M., Laso M., Numerical simulation of 3D viscoelastic flows with free surfaces, Journal of Computational Physics, 215, 691-716, 2006.
[7] Tryggvason G., Bunner B., Esmaeeli A., Juric D., Al-Rawahi N., Tauber W., Han J., Nas S., Jan Y.-J., A front-tracking method for the computations of multiphase flow, Journal of Computational Physics, 169, 708-759, 2001.
[8] Bird R.B., Wiest J.M., Constitutive equations for polymeric liquids, Annual Review of Fluid Mechanics, 27, 169-193, 1995.
[9] Alves M.A., Oliveira P.J., Pinho F.T., A convergent and universally bounded interpolation scheme for the treatment of advection, International Journal for Numerical Methods in Fluids, 41, 47-75, 2003.
[10] Keunings R., On the high Weissenberg number problem, Journal of Non-Newtonian Fluid Mechanics, 20, 209-226, 1986.
[11] Fattal R., Kupferman R., Constitutive laws for the matrix-logarithm of the conformation tensor, Journal of Non-Newtonian Fluid Mechanics, 123, 281-285, 2004.
[12] Fattal R., Kupferman R., Time-dependent simulation of viscoelastic flows at high Weissenberg number using the log-conformation representation, Non-Newtonian Fluid Mechanics, 126, 23-37, 2005.
[13] Alves M.A., Pinho F.T, Oliveira P.J., Effect of a high-resolution differencing scheme on finite-volume predictions of viscoelastic flows, Journal of Non-Newtonian Fluid Mechanics, 93, 287-314, 2000.
[14] Perot J.B., An analysis of the fractional step method, Journal of Computational Physics, 108, 51-58, 1993.
[15] Pilliod J.E., Puckett E.G., Second-order accurate volume-of-fluid algorithms for tracking material interfaces, Journal of Computational Physics, 199, 465-502, 2004.
[16] Hayat T., Khan M., Ayub M., Exact solutions of flow problems of an Oldroyd-B fluid, Applied Mathematics and Computation, 151, 105-119, 2004.
[17] Hinch E.J., The flow of an Oldroyd-B fluid around a sharp corner, Journal of Non-Newtonian Fluid Mechanics, 50, 161-171, 1993.
[18] Davies A.R., Devlin J,, On corner flows of Oldroyd-B fluids, Journal of Non-Newtonian Fluid Mechanics, 50, 173-191, 1993.
[19] Aboubacar M., Matallah H., Webster M.F., Highly elastic solutions for Oldroyd-B and Phan-Thien/Tanner fluids with a finite volume/element method: planar contraction flows, Journal of Non-Newtonian Fluid Mechanics, 103, 65-103, 2002.
[20] Alves M.A., Oliveira P.J., Pinho F.T., Benchmark solutions for the flow of Oldroyd-B an PTT fluids in planar contractions, Journal of Non-Newtonian Fluid Mechanics, 110, 45-75, 2003.